Convolution-in-time approximations of time domain boundary integral equations

SIAM J. SCI. COMPUT.
Vol. 35, No. 1, pp. B43–B61

CONVOLUTION-IN-TIME APPROXIMATIONS OF TIME DOMAIN BOUNDARY INTEGRAL EQUATIONS*

PENNY J. DAVIES† AND DUGALD B. DUNCAN‡

Abstract. We present a new temporal approximation scheme for the boundary integral formulation of time-dependent scattering problems which can be combined with either collocation or Galerkin approximation in space. It uses the backward-in-time framework introduced in [P. J. Davies and D. B. Duncan, *Convolution Spline Approximations of Volterra Integral Equations*, www.mathstat.strath.ac.uk/research/reports/2012 (2012)] with new temporal basis functions which share some properties with radial basis function multiquadrics. We analyze the stability and convergence properties of the new scheme for associated Volterra integral equations and perform extensive numerical tests for scattering from flat polygonal plates and open and closed cubes and spheres, which demonstrate effectiveness of this approach.

Key words. convolution quadrature, Volterra integral equations, time-dependent boundary integral equations

AMS subject classifications. 65R20, 65M12

DOI. 10.1137/120881907

1. Introduction.

The focus of this paper is to develop, analyze, and test approximation methods for the time-dependent boundary integral equation (TDBIE)

$$\frac{1}{4\pi}\int_\Gamma \frac{u(\boldsymbol{x}',t-|\boldsymbol{x}'-\boldsymbol{x}|)}{|\boldsymbol{x}'-\boldsymbol{x}|}\,d\boldsymbol{x}' = a(\boldsymbol{x},t) \quad \text{for } \boldsymbol{x}\in\Gamma,\ t>0\,. \tag{1.1}$$

This is the single layer potential equation for acoustic scattering from the surface $\Gamma \subset \mathbb{R}^3$ with zero Dirichlet boundary condition: $-a(\boldsymbol{x},t)$ is the (known) incident field, and the problem is to compute the induced surface potential u (see, e.g., [10] for more details). It has been shown [1, 9, 15] that when Γ is a smooth, closed or open, flat surface, then (1.1) is well-posed and a full Galerkin approximation in time and space is stable and convergent. However, the stability of the method relies on all the integrals being evaluated extremely accurately (as described in [19]). We previously analyzed collocation approximations of (1.1) in [6] and demonstrated their stability when $\Gamma = \mathbb{R}^2$, but this also requires all surface integrals to be evaluated very accurately.

Lubich proved in [15] that a spatial Galerkin approximation of (1.1) which uses convolution quadrature (CQ) in time (based on an underlying linear multistep ODE solver) is convergent. A key difference is that this method is stable when the inner product integrals are approximated, i.e., using CQ in time is inherently far more stable than using Galerkin or collocation time approximations. The drawback is that the underlying basis functions are global, which significantly increases the computational complexity of the method, even when a careful cutoff strategy is used to sparsify

*Submitted to the journal's Computational Methods in Science and Engineering section June 20, 2012; accepted for publication (in revised form) November 13, 2012; published electronically January 8, 2013.

http://www.siam.org/journals/sisc/35-1/88190.html

†Department of Mathematics and Statistics, University of Strathclyde, 26 Richmond Street, Glasgow, G1 1XH, UK (penny.davies@strath.ac.uk).

‡Maxwell Institute for Mathematical Sciences, Department of Mathematics, Heriot–Watt University, Edinburgh, EH14 4AS, UK (D.B.Duncan@hw.ac.uk).

the system matrices [11, 13]. CQ methods which are based on underlying Runge–Kutta ODE solvers have been developed and analyzed for TDBIEs in [3, 4]. There are several advantages of these methods over linear multistep CQ methods: higher order accurate methods in time are possible, and the basis functions are more highly concentrated (see [2, Figures 1–2] and Figure 2.2 below), which makes sparsifying the system matrices more straightforward. Banjai uses this approach in [2] to develop a practical, parallelizable solution algorithm for (1.1) which he illustrates with a number of realistic large-scale numerical examples.

In [7] we considered an alternative approach, developing a new "convolution spline" method which shares some properties of CQ, but instead of being based on an underlying ODE solver it is explicitly constructed in terms of basis functions which have compact support. Although (1.1) was the motivation for [7], the analysis is for the convolution-kernel Volterra integral equation (VIE)

$$\int_0^t K(t')\,u(t-t')\,dt' = a(t) \quad \text{for } t \in [0,T]\,, \quad \text{where } a(0)=0,\ K(0)=1\,. \tag{1.2}$$

The connection is that if $\Gamma = \mathbb{R}^2$, then the spatial Fourier transform of (1.1) at frequency $\boldsymbol{\omega} \in \mathbb{R}^2$ is the VIE

$$\int_0^t J_0(\omega t')\,\widehat{u}(\boldsymbol{\omega}, t-t')\,dt' = 2\,\widehat{a}(\boldsymbol{\omega}, t)\,,$$

where $\omega = |\boldsymbol{\omega}|$ and J_0 is the first kind Bessel function of order zero.

A key feature of the method of [7] is that it uses the CQ backward-in-time format. That is, the solution u of (1.2) at time $t = t_n = nh$ is approximated as

$$u(t_n - t') \approx \sum_{j=0}^{n} v_{n-j}\,\phi_j(t'/h) \quad \text{for } t' \geq 0 \tag{1.3}$$

in terms of B-spline basis functions ϕ_j, where v_j approximates $u(t)$ for t near t_j. As noted in [7] this type of approximation is fundamentally different from finite element type methods in which the basis function ϕ_j is always associated with the same "unknown" v_j. Here we also consider approximations of the form (1.3) but using nonpolynomial basis functions ϕ_j, which give more stable numerical schemes when applied to the full TDBIE problem (1.1).

We begin in section 2 with a description of the key approximation properties of the new basis functions, and in section 3 we prove that the approximate solution (1.3) converges to the exact solution of the VIE (1.2) when K and a are smooth and is stable when K is constant or a step-function. (Stability in these cases is important for stability of approximations of the TDBIE (1.1) which uses (1.3) in time.) We explain in section 4 how this method can be used as the temporal approximation of the TDBIE (1.1) and give the results of extensive numerical tests which illustrate the effectiveness of this approach together with both Galerkin and collocation approximations in space. We consider scattering from a flat polygonal plate (i.e., a screen problem), an open and closed cube, and a closed sphere. The spatial Galerkin approximation appears to give rise to a stable numerical scheme in all these examples, and the spatial collocation approximation appears stable in all cases apart from the sphere. We end with some preliminary results for a related temporal approximation which uses smooth, compact basis functions and appears to give a stable TDBIE scheme even in the case of spatial collocation on the sphere.

2. Convolution basis in time approximation. We begin by describing the approximation scheme for the VIE (1.2). Note that if

$$a \in C^{d+1}[0,T] \quad \text{and} \quad K \in C^{d+1}[0,T] \tag{2.1}$$

for some $d \geq 0$, then (1.2) has a unique solution $u \in C^d[0,T]$ (see, e.g., [5, Theorem 2.1.9]). For simplicity we restrict attention to the case for which the extension of the solution u by zero to the negative real axis is in $C^d(-\infty,T]$. (Otherwise the method needs to be "corrected" as described for CQ in [14, section 3] in order to attain optimal convergence.) If (2.1) holds or K is a step-function, then this is guaranteed by requiring

$$a^{(p)}(0) = 0 \quad \text{for } p = 0 : d+1 \tag{2.2}$$

because $u^{(p)}(0) = a^{(p+1)}(0) - \sum_{\ell=0}^{p-1} K^{(p-\ell)}(0)\, u^{(\ell)}(0)$.

2.1. Approximating the VIE (1.2). The approximation is defined on a uniform grid with spacing h. At $t = t_n := nh$ for $n \leq N_T := \lfloor T/h \rfloor$, (1.2) can be written as

$$\int_0^\infty K(t')\, u(t_n - t')\, dt' = a(t_n)\,, \tag{2.3}$$

because $u(t) = 0$ for $t \leq 0$, and the main feature of the convolution basis in time approach is to use (1.3) to approximate u in (2.3). Collocating in time then gives the approximation scheme

$$\sum_{j=0}^{n} q_j\, v_{n-j} = a(t_n) \quad \text{for } n = 0 : N_T \tag{2.4}$$

for the unknowns v_j, where the weights q_j are defined by

$$q_j = \int_0^\infty K(t)\, \phi_j(t/h)\, dt\,.$$

The v_j can be found by time marching in (2.4): $v_n = (a(t_n) - \sum_{j=0}^{n-1} q_j\, v_{n-j})/q_0$ for $n \geq 1$ (using $v_0 = 0$). An alternative expression which is useful for analysis is $v_n = (\sum_{j=0}^{n} p_j\, a(t_{n-j}))/q_0$ for $n \geq 1$, where the stability coefficients p_n are defined recursively by

$$p_0 = 1\,, \quad p_n = \frac{-1}{q_0} \sum_{j=1}^{n} q_j\, p_{n-j} \quad \text{for } n \geq 1\,. \tag{2.5}$$

2.2. Basis functions. We consider a class of smooth quasi-interpolant basis functions ϕ_j which approximate hat functions (linear B-splines) and fit into the framework described in [21] for radial basis function multiquadrics when adapted to a semi-infinite interval. They are derived in terms of an "underlying" function $\psi(t)$ as follows:

$$\left.\begin{aligned} \phi_0(t) &= [\,\psi(t-1) + 1 - t\,]/2 \\ \phi_1(t) &= [\,\psi(t-2) - 2\,\psi(t-1) + t\,]/2 \\ \phi_j(t) &= [\,\psi(t-j-1) - 2\,\psi(t-j) + \psi(t-j+1)\,]/2 \quad \text{for } j \geq 2 \end{aligned}\right\}. \tag{2.6}$$

Note that this choice of terminology is consistent with [7], but ϕ and ψ are used the opposite way around in [21].

Careful choice of ψ gives good approximation properties, and in particular we assume the following.

DEFINITION 2.1. *The function $\psi : \mathbb{R} \to \mathbb{R}$ is smooth, even (i.e., $\psi(-t) = \psi(t)$), and positive and behaves like $|t|$ at infinity. More precisely,*

$$\begin{aligned} &\exists\ C_0,\ C_1 \text{ and } M \text{ such that } \left|t - \psi(t) + C_0\, t^{-1}\right| \le C_1\, t^{-2} \quad \text{for } t > M, \\ &\lim_{t\to\infty} \psi'(t) = 1, \\ &\psi''(t) > 0 \quad \text{for all } t \in \mathbb{R}, \text{ and } \lim_{t\to\infty} \psi''(t) = 0\,. \end{aligned} \tag{2.7}$$

We focus attention on a particular choice of ψ in section 2.3 but begin with some general results for any basis functions ϕ_j which fit into the framework (2.6). Note that (2.7) implies the following:

$$\left.\begin{aligned} &\lim_{x\to\infty} (\psi(x+1) - \psi(x)) = 1 \\ &\lim_{x\to\infty} (x\,\psi(x+1) - (x+1)\,\psi(x)) = 0 \end{aligned}\right\}. \tag{2.8}$$

LEMMA 2.1. *If ψ satisfies the properties of Definition* 2.1, *then the basis functions ϕ_j satisfy the sum to unity property*

$$\sum_{j=0}^{\infty} \phi_j(t) \equiv 1 \quad \text{and also} \quad \sum_{j=0}^{\infty} j\,\phi_j(t) = t \quad \text{for all } t \in \mathbb{R}\,.$$

Proof. Set $S_N^m(t) = \sum_{j=0}^{N} j^m\,\phi_j(t)$ for $m = 0:1$. Then it can be shown (because ψ is even) that

$$\begin{aligned} S_N^0(t) &= (1 + \psi(N+1-t) - \psi(N-t))\,/2\,, \\ S_N^1(t) &= (t + N\psi(N+1-t) - (N+1)\psi(N-t))\,/2\,. \end{aligned}$$

Taking the limit as $N \to \infty$ using (2.8) then gives the required results, since

$$\begin{aligned} &N\psi(N+1-t) - (N+1)\psi(N-t) \\ &\quad = t\,(\psi(N+1-t) - \psi(N-t)) \\ &\qquad + (N-t)\,\psi(N-t+1) - (N-t+1)\,\psi(N-t)\,. \end{aligned}$$

∎

We make frequent use of the following formula for the mth difference of a function f.

LEMMA 2.2. *Let δ_h^m denote the mth forward difference with spacing h, i.e.,*

$$\delta_h^m\, f_j := \sum_{k=0}^{m} (-1)^{m-k} \left(\begin{array}{c} m \\ k \end{array} \right) f_{j+k}\,,$$

where $f_j = f(t_j)$. Then if f is smooth,

$$\delta_h^m\, f_j = h^{m-1} \int_0^{mh} f^{(m)}(t_j + s)\, b_{m-1}(s/h)\, ds, \tag{2.9}$$

where b_ℓ is the ℓth degree B-spline defined recursively by

$$b_0(\tau) = \begin{cases} 1 & \text{if } \tau \in [0,1), \\ 0 & \text{otherwise,} \end{cases} \qquad \text{and if } \ell \ge 1\text{: } b_\ell(\tau) = \frac{\tau}{\ell}\, b_{\ell-1}(\tau) + \frac{\ell + 1 - \tau}{\ell}\, b_{\ell-1}(\tau - 1)\,.$$

Proof. See, e.g., [20, Chapter 7] for a derivation of (2.9) (in slightly different notation). ∎

The next two results are an immediate consequence of (2.9).

COROLLARY 2.1. *If f is smooth and satisfies $f^{(m)}(t) \geq 0$ for $t \in (t_j, t_{j+m})$, then $\delta_h^m f_j \geq 0$.*

COROLLARY 2.2. *If ψ satisfies the properties of Definition* 2.1*, then $\phi_j(t) \geq 0$ for $j \geq 2$.*

The final result of this subsection shows that quasi-interpolation in terms of the basis ϕ_j inherits useful approximation properties.

LEMMA 2.3. *Let $\mathcal{L}f(t)$ denote the quasi-interpolant of the function f in terms of the basis functions ϕ_j on a uniform mesh with spacing h, i.e.,*

$$\mathcal{L}f(t) = \sum_{j=0}^{\infty} f_j \, \phi_j(t/h) \, ,$$

where $f_j = f(jh)$. Then

(i) *the operator $\mathcal{L}$ preserves linearity;*

(ii) *if f is a bounded function, then so is $\mathcal{L}f$;*

(iii) *if ψ behaves well enough at infinity for $\sum_{j=0}^{\infty} |\phi_j^{(m)}| < \infty$ when $m = 1 : 2$, then $\mathcal{L}$ also preserves convexity and monotonicity (for sufficiently smooth f).*

Proof. Linearity follows immediately from Lemma 2.1, and boundedness of $\mathcal{L}f$ is a consequence of the sum to unity property from Lemma 2.1, Corollary 2.2, and (2.7). The proof of convexity and monotonicity follows [21], although the sums involved are now infinite. For example, if $f \in C^2[0, \infty)$ is convex, then Corollary 2.1 gives $\delta_h^2 f_j > 0$ and

$$(\mathcal{L}f)''(t) = \frac{1}{2\,h^2} \sum_{j=0}^{\infty} \psi''(t/h - j) \, \delta_h^2 f_j > 0 \, . \qquad \blacksquare$$

2.3. Particular choice of basis functions. The particular basis functions we analyze and use for most of the numerical test results are ϕ_j derived from the underlying function

$$\psi(t) = t \, \mathrm{erf}(\alpha t) + \frac{1}{\alpha\sqrt{\pi}} \, e^{-\alpha^2 t^2} \, , \tag{2.10}$$

where erf is the error function [8, 8.250] and $\alpha \geq 1$ is a constant. Note that

$$\psi'(t) = \mathrm{erf}(\alpha \, t) \in (-1, 1) \, , \quad \psi''(t) = \frac{2\,\alpha}{\sqrt{\pi}} \, e^{-\alpha^2 t^2} > 0 \quad \text{for all } t \in \mathbb{R}$$

and it is straightforward to verify that ψ satisfies all the properties of Definition 2.1 and Lemma 2.3. We now collect together some extra results which are needed in section 3.

LEMMA 2.4. *The function ψ from* (2.10) *and the corresponding basis functions ϕ_j satisfy the following:*

P1. *Linear approximation,*

$$| \, |t| - \psi(t) \, | \leq \frac{1}{\alpha\sqrt{\pi}} \, e^{-\alpha^2 t^2} .$$

P2. *Basis function bound. If* $t > j+1$, *then*

$$|\,\phi_j(t)\,| \le \frac{2}{\alpha\sqrt{\pi}}\, e^{-\alpha^2(t-j-1)^2}. \tag{2.11}$$

P3. *Basis function positivity. Each* ϕ_j *for* $j \neq 1$ *is positive on* $[0,\infty)$.

P4. *Basis function integral. Let*

$$J := \frac{1}{2}\int_0^\infty (\psi(t)-t)\; dt = \frac{1}{8\,\alpha^2} \quad \textit{and}$$

$$I(j) := \frac{1}{2}\int_0^j (\psi(t)+t)\; dt = \frac{j^2}{4}\,(\mathrm{erf}(\alpha\, j)+1) + \frac{j\, e^{-j^2\alpha^2}}{4\,\alpha\sqrt{\pi}} + \frac{\mathrm{erf}(\alpha\, j)}{8\,\alpha^2}$$

for $j \ge 0$*; then*

$$\int_0^\infty \phi_j(t)\, dt = \begin{cases} I(1)+J & \textit{for } j=0, \\ I(2)-2\,I(1)-J & \textit{for } j=1, \\ I(j+1)-2\,I(j)+I(j-1) & \textit{for } j \ge 2\,. \end{cases}$$

P5. *Translate property. The basis functions* ϕ_j *for* $j \ge 2$ *are translates, i.e.,* $\phi_j(t) = \Phi(t-j)$, *where*

$$\Phi(t) := [\psi(t+1) - 2\,\psi(t) + \psi(t-1)\,]/2$$

is symmetric (even) and positive. In addition $\Phi(t)$ *has a global maximum at* $t=0$ *and is monotonic decreasing for* $t > 0$.

Proof. Properties P1 and P2 follow from the Mills' ratio bound of [16, section 7.8], which implies

$$x\;(1-\mathrm{erf}(x)\,) \le \frac{2\,e^{-x^2}}{\sqrt{\pi}} \quad \text{for all } x > 0\,. \tag{2.12}$$

This result also implies that $\phi_0(t) > 0$ when $t \ge 0$, and Corollary 2.2 gives positivity of ϕ_j for $j \ge 2$. Note that although $\phi_1(t)$ is negative at $t=0$, it is positive for $t > t_\alpha$, where t_α is small (and $t_\alpha \to 0$ as $\alpha \to \infty$). The bound (2.11) shows that each $\phi_j \in L^1(0,\infty)$, and direct computation of the integrals yields P4. Finally, it is straightforward to verify that the function Φ of P5 satisfies $\Phi'(0) = 0$ and $\Phi''(0) < 0$. If $\Phi'(t) > 0$ for some $t > 0$, then there must be a value of $t_* > 0$ at which $\Phi''(t_*) = 0$ and $\Phi'''(t_*) \le 0$, and it can be shown by comparing these expressions that this is impossible, and so $\Phi'(t) \le 0$ when $t > 0$. ∎

The basis functions ϕ_j are illustrated in Figure 2.1 and their width of support is compared with that of the corresponding BDF2 and RK convolution quadrature basis functions in Figure 2.2. The ϕ_j are much more compact and, since they are translates, do not get wider as j increases, unlike the BDF2 and RK schemes.

2.4. Other basis functions. We also present some preliminary computational results for an approximation scheme which uses basis functions which are globally C^∞ and have compact support (of width 4). They fit into the framework of (2.6) and are constructed from the smooth underlying function

$$\tilde{\psi}(t) = \begin{cases} t\,\mathrm{erf}(2\tanh^{-1}(t)) + \frac{1}{2\sqrt{\pi}}\,\exp(-4[\tanh^{-1}(t)]^2) & \text{for } |t| < 1, \\ |t| & \text{for } |t| \ge 1\,. \end{cases} \tag{2.13}$$

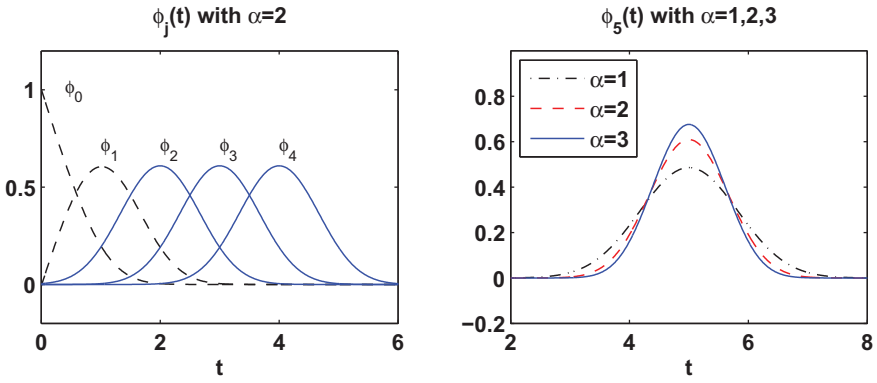

FIG. 2.1. *Basis functions $\phi_j(t)$. The right-hand plot shows the dependence on the parameter α.*

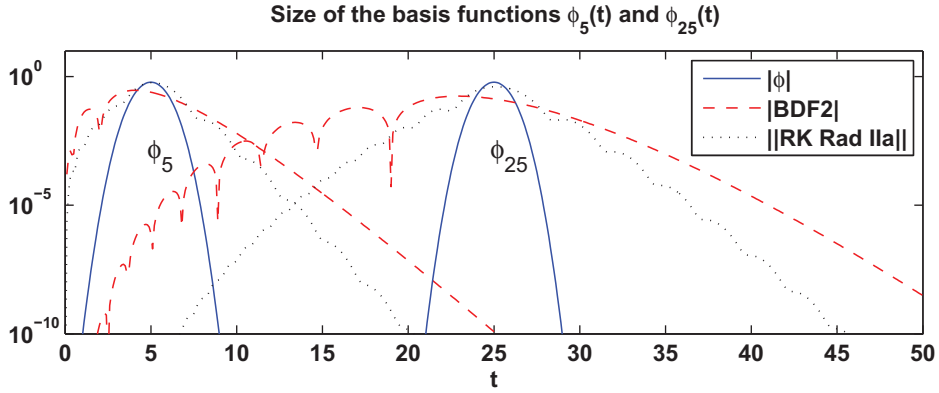

FIG. 2.2. *Size of the basis functions ϕ_5 and ϕ_{25} with $\alpha = \sqrt{2}$ compared with the corresponding BDF2 convolution quadrature basis functions and the matrix 2-norm of the 2×2 basis function matrix for the two-stage RK Radau IIa method of* [2, Figure 2].

There is clearly scope to parameterize the function $\tilde{\psi}$ to modify its shape and width. Smooth, compact temporal basis functions have also been considered for a full space-time Galerkin approximation of (1.1) in [17].

Note that linear B-spline basis functions can be constructed in the same way in terms of the underlying function $\psi(t) = |t|$, and we use this observation when bounding the approximation error.

3. Stability and convergence of the VIE approximation. We now analyze the backward-in-time approximation (1.3) of the VIE (1.2). We first prove that it is stable (in the sense used in [7]) when K is constant or a step-function—this is necessary for stability of approximations of the TDBIE (1.1), which uses (1.3) in time—and then show that it converges at rate $\mathcal{O}(h^2)$ when a and K are smooth.

3.1. Stability of the VIE approximation. As in [7] we require the approximation scheme for (1.2) to be stable in the following sense, independent of the input function $a(t)$.

DEFINITION 3.1 (stability). *The scheme* (1.3) *is said to be stable when the impulse response sequence $\{p_n\}$ defined by* (2.5) *satisfies $|p_n| \leq C$ for all n such that $t_n \leq T$, where the constant C is independent of h.*

We now derive sufficient conditions for stability and show how they can be applied in some special cases.

3.1.1. Sufficient conditions for stability. Taking the first and second differences of (2.5) gives, respectively,

$$q_0\, p_{n+1} + \sum_{j=0}^{n} (q_{j+1} - q_j)\; p_{n-j} = 0 \quad \text{and} \tag{3.1}$$

$$q_0\, p_{n+2} + (q_1 - 2\, q_0)\, p_{n+1} + \sum_{j=0}^{n} (q_{j+2} - 2\, q_{j+1} + q_j)\; p_{n-j} = 0\,. \tag{3.2}$$

Each of these expressions can be used to prove stability under suitable conditions on the coefficients q_j, as summarized below.

THEOREM 3.1. *Suppose that*

$$q_0 > 0\,, \quad q_{j+1} - q_j \geq 0 \text{ for } j \geq 2 \tag{3.3}$$

and either

$$q_{j+1} - q_j \geq 0 \text{ for } j = 0:1 \quad \text{and} \quad q_j - q_0 \leq q_0 \text{ for } j \geq 2 \tag{3.4}$$

or

$$q_1 - 2\, q_0 \leq 0 \quad \text{and} \quad q_{j+1} - 2\, q_j + q_{j-1} \leq 0 \text{ for } j \geq 1\,. \tag{3.5}$$

Then for all $n \geq 0$*,*

$$|p_n| \leq \max\{1, |q_1|/q_0\}\,. \tag{3.6}$$

Proof. By definition, $p_0 = 1$ and $p_1 = -q_1/q_0$, and so (3.6) holds for $n = 0:1$. Suppose first that (3.4) holds; then using the triangle inequality in (3.1) with $n \geq 1$ and (3.3) gives

$$|p_{n+1}| \leq \sum_{j=0}^{n} \left(\frac{q_{j+1} - q_j}{q_0}\right) |p_{n-j}| \leq \max_{j=0:n} |p_j| \left(\frac{q_{n+1} - q_0}{q_0}\right) \leq \max_{j=0:n} |p_j|,$$

and so (3.6) holds for all n by induction.

It can similarly be shown by using the triangle inequality for (3.2) that if (3.5) holds, then

$$|p_{n+2}| \leq \left(\frac{q_0 + q_{n+1} - q_{n+2}}{q_0}\right) \max_{j=0:n+1} |p_j| \leq \max_{j=0:n+1} |p_j|\,,$$

and so (3.6) is satisfied for all n in this case too. ∎

3.1.2. Stability when $K(t) \equiv 1$. In this case

$$q_j = h \int_0^\infty \phi_j(t)\, dt$$

and these integrals are given in P4 of Lemma 2.4. In order to prove stability it is sufficient to verify that the coefficients satisfy the conditions of Theorem 3.1. In fact

they satisfy (3.3) and both (3.4) and (3.5) for suitable values of α. We verify this below because all these inequalities are needed in subsequent analysis: formulation (3.1) (which needs (3.4)) is used in the following subsection and formulation (3.2) (which needs (3.5)) is used in the convergence proof of section 3.2.

LEMMA 3.1. *The coefficients q_j when $K \equiv 1$ satisfy* (3.3) *for all $\alpha > 0$,* (3.4) *when $\alpha \geq 1$, and* (3.5) *when $\alpha > 1.2$.*

Proof. Property P3 of Lemma 2.4 gives $q_0 > 0$, and it follows from P4 that if $j \geq 2$, then $q_{j+1} - q_j = h\,\delta_1^3\, I(j-1)$. This is positive by Corollary 2.1 because $I^{(3)}(x) = \psi''(x)/2 > 0$. Similarly, $q_2 - q_1 = h\,\delta_1^3\, I(0) + J > 0$, and

$$\frac{q_1 - q_0}{h} = I(2) - 3\,I(1) - J$$

can be shown to be positive for all $\alpha \geq 1$. Thus for any $\alpha \geq 1$, the sequence $\{q_j\}$ is monotonic increasing in j, and we can use Lemma 2.2 to calculate the limiting behavior: $q_{j+1} = h\,\delta_1^2\, I(j)$, where

$$\delta_1^2\, I(j) = \int_0^2 I''(j+s)\, b_1(s)\, ds = \frac{1}{2} \int_0^2 [1 + \psi'(j+s)\,]\; b_1(s)\, ds \to 1 \quad \text{as } j \to \infty\,.$$

So for any $j \geq 1$,

$$\frac{q_j - 2\,q_0}{h} \leq 1 - 2\;(I(1) + J) < (1 - \operatorname{erf}\alpha)\,/2 - (1 + \operatorname{erf}\alpha)\,/(4\alpha^2),$$

which is negative for $\alpha \geq 1$, which verifies the second inequality of (3.4) and the first of (3.5). For the final part of (3.5),

$$q_{j+1} - 2\,q_j + q_{j-1} = h\,\delta_1^4\, I(j-2) < 0 \quad \text{when } j \geq 3$$

because $I^{(4)}(x) = \psi^{(3)}(x)/2 < 0$, and $q_3 - 2\,q_2 + q_1 = h\,\left(\delta_1^4\, I(0) - J\right) < 0$. The restriction $\alpha > 1.2$ is necessary for the final inequality: $I(j) \to j^2/2$ and $J \to 0$ as $\alpha \to \infty$, and so

$$(q_2 - 2\,q_1 + q_0)\,/h \to -1/2\,.$$

Hence the term is negative when α is sufficiently large, and it is straightforward to verify that $\alpha \geq 1.2$ is sufficiently large. ∎

Remark. Theorem 3.1 does not give an optimal bound on the size of p_n when $K \equiv 1$. In fact it can be shown that $|p_n| \leq C\,\lambda^n$ for constants $\lambda \in (0,1)$ and C which are independent of h.

3.1.3. Step-function kernel. We now consider (1.2) with discontinuous kernel K_L given by

$$K_L(t) = \begin{cases} 1 & \text{when } t \in [0, L], \\ 0 & \text{for } t > L\,, \end{cases}$$

where the duration L is independent of h.

Remark. The TDBIE problem for scattering from the unit sphere for which u is constant in space is the VIE (1.2) with $K = K_2$ [18], so stability for a VIE with a step-function kernel is necessary for good behavior of (1.1) when Γ is a smooth, closed surface.

The stability proof for the step-function kernel is similar to Theorem 3.1, but now the sequence $\{q_j\}$ increases to a peak at $j \approx L/(2h)$ and then decreases, and the coefficients p_n are no longer bounded by q_1/q_0.

THEOREM 3.2. *When $K = K_L$ the coefficients q_j are all positive and satisfy the following inequalities for sufficiently small h:*

$$q_{j+1} - q_j > 0 \quad \text{for } j = 0 : J_L\,, \quad q_{j+1} - q_j < 0 \quad \text{for } j > J_L, \quad \text{and} \quad q_{J_L} < 2\,q_0\,, \tag{3.7}$$

where $J_L = \lfloor \frac{L-h}{2\,h} \rfloor$.

Under these conditions the approximation scheme (1.3) *is stable in the sense of Definition* 3.1.

Proof. We showed that both $q_1 - q_0$ and $q_2 - q_1$ are positive when $K \equiv 1$ in Lemma 3.1, and so this also holds for K_L when h is sufficiently small. When $j \geq 2$ we use P5 of Lemma 2.4 and write $\phi_j(t) = \Phi(t - j)$. Then

$$q_{j+1} - q_j = \int_0^1 \left[\, \Phi(t + j) - \Phi(t + L/h - j - 1) \,\right] dt$$

and it follows from the monotonicity of Φ that $\Phi(t + L/h - j - 1) \leq \Phi(t + j)$ if and only if $L/h - j - 1 \geq j$, which gives the first two inequalities. The proof of the final inequality is similar to that for $K \equiv 1$: we have $2\,q_0 - q_{J_L} > 2\,q_0 - 1$, which is positive for sufficiently small h.

We now use (3.1) to show that conditions (3.7) are sufficient to guarantee stability. A similar argument to that used in Theorem 3.1 gives $|p_n| \leq q_1/q_0$ for $n = 0 : J_L$, and so $\rho_k = q_1/q_0$ for $k = 1 : J_L$, where we define $\rho_k := \max_{j=0:k} |p_j|$. Note that the sequence $\{\rho_k\}$ is positive and montonically increasing in k, and if $n > J_L$, then $\rho_k \leq \rho_{n-J_L}$ for $k = 0 : J_L$.

If $n > J_L$ and $k = J_L : n$, then it follows from (3.7) and the triangle inequality for (3.1) that

$$\begin{aligned}
|p_{k+1}| &\leq \sum_{j=0}^{J_L-1} \frac{q_{j+1} - q_j}{q_0}\, |p_{k-j}| + \sum_{j=J_L}^{k} \frac{q_j - q_{j+1}}{q_0}\, |p_{k-j}| \\
&\leq \rho_n \sum_{j=0}^{J_L-1} \frac{q_{j+1} - q_j}{q_0} + \rho_{n-J_L} \sum_{j=J_L}^{k} \frac{q_j - q_{j+1}}{q_0} \\
&= \theta\,\rho_n + (\theta + 1 - q_{n+1}/q_0)\;\rho_{n-J_L}\,,
\end{aligned}$$

where $\theta = (q_{J_L} - q_0)/q_0 \in (0, 1)$. Thus $|p_{k+1}| \leq \theta\,\rho_n + (\theta + 1)\;\rho_{n-J_L}$ for $k = 0 : n$, and hence

$$\rho_{n+1} \leq \theta\,\rho_n + (1 + \theta)\,\rho_{n-J_L} \quad \text{when } n > J_L.$$

It can be shown by induction that this implies

$$\rho_n \leq \gamma^{\frac{n}{J_L+1}}, \quad \text{where } \gamma = \left(\frac{1+\theta}{1-\theta}\right)$$

—if true up to n, then

$$\rho_{n+1} \leq \theta\,\gamma^{\frac{n}{J_L+1}} + (1 + \theta)\,\gamma^{\frac{n-J_L}{J_L+1}} = \theta\,\gamma^{\frac{n}{J_L+1}} + (1 - \theta)\,\gamma^{\frac{n+1}{J_L+1}},$$

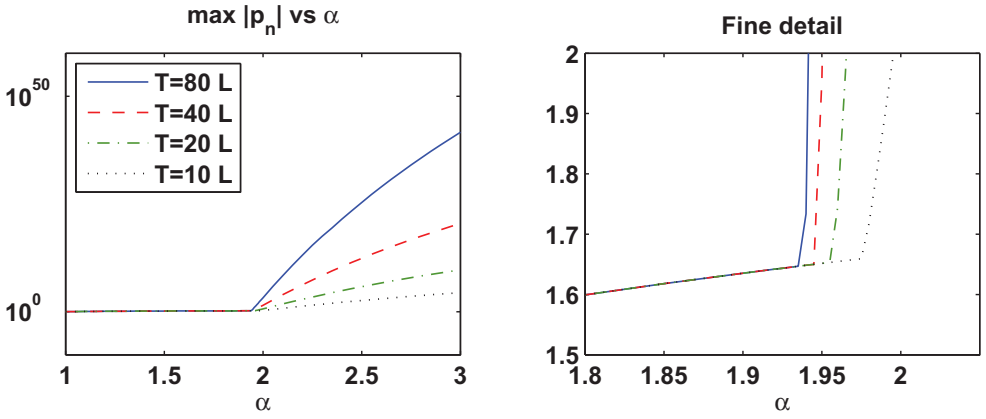

FIG. 3.1. *Plots of* $\max_n |p_n|$ *against the width parameter* α *when* $K = K_L$*. In these examples* L *is half-way between two time-levels (i.e.* $2L/h$ *is an odd integer) which appears to be the worst case for growth. The plots show that when* $\alpha < 1.9$ *then* $|p_n| \le q_1/q_0$*, but for larger* α *then there is growth of the form* $\lambda^{T/L}$ *as given by the bound* (3.8) *of Theorem* 3.2.

which gives the required bound. That is,

$$|p_n| \le \left(\frac{1+\theta}{1-\theta}\right)^{\frac{n}{J_L+1}} \le \left(\frac{1+\theta}{1-\theta}\right)^{\frac{2T}{L}} . \tag{3.8}$$

Note that although extremely large, this bound is independent of h and so the scheme is stable. □

The growth factor in the bound (3.8) is unduly pessimistic for moderate values of α (smaller than about 1.9), although the maximum value of $|p_n|$ can be very large at other values of α, as illustrated in Figure 3.1.

3.2. Convergence of the VIE approximation. The approximation error for (1.3) at time $t \ge 0$ is

$$e_n(t) = u(t_n - t) - \sum_{j=0}^{n} v_{n-j}\, \phi_j(t/h)\,, \tag{3.9}$$

where u is the exact solution of (1.2) and the coefficients v_j satisfy (2.4). We now state and prove the main result of this section.

THEOREM 3.3. *If* (2.1) *and* (2.2) *hold for* $d \ge 4$ *and* $\alpha > 1.2$*, then there is a constant* C *independent of* h *(but depending on* T*) such that*

$$|e_n(t)| \le C\, h^2 \tag{3.10}$$

when $t \in [0, t_n]$ *for each* $n \le N_T = \lfloor T/h \rfloor$*.*

Proof. Note that (3.10) trivially holds for $t \le t_1$ because (2.1) and (2.2) imply that $u(ch) = \mathcal{O}(h^d)$ for any constant c. For $t > t_1$ we follow the same procedure as [7, Theorem 4.1], but the situation here is more complicated because the basis functions are global. The first stage is to show that $e_n(t)$ can be expressed in terms of coefficients $\varepsilon_k = u(t_k) - v_k$ up to $\mathcal{O}(h^2)$. Let $\widehat{\phi}_j$ denote the linear B-spline basis functions derived

using the construction (2.6) starting from $\widehat{\psi}(t) = |t|$; then rearranging (3.9) gives

$$\left| e_n(t) - \sum_{j=0}^{n} \varepsilon_{n-j}\, \phi_j(\tfrac{t}{h}) \right| \le \left| u(t_n - t) - \sum_{j=0}^{n} u(t_{n-j})\, \widehat{\phi}_j(\tfrac{t}{h}) \right| + \left| \sum_{j=0}^{n} u(t_{n-j})\, \left(\widehat{\phi}_j(\tfrac{t}{h}) - \phi_j(\tfrac{t}{h}) \right) \right|.$$

The first term on the right is the error in linear interpolation and so is bounded by $\mathcal{O}(h^2)$, while the second can be written as

$$\left| \frac{1}{2} \sum_{j=1}^{n-1} \left(\widehat{\psi}(\tfrac{t}{h} - j) - \psi(\tfrac{t}{h} - j) \right) \delta_h^2\, u(t_{n-j-1}) + \left(\widehat{\psi}(\tfrac{t}{h} - t_n) - \psi(\tfrac{t}{h} - t_n) \right) \frac{u(t_1)}{2} \right| \le C\, h^2 \sum_{j=1}^{n-1} e^{-\alpha^2 (t/h - j)^2} + \mathcal{O}(h^3)$$

using P1 of Lemma 2.4 and $\delta_h^2\, u(t_{n-j-1}) = h^2\, u''(t_n - j) + \mathcal{O}(h^4)$ (for δ_h^2 as defined in Lemma 2.2). Hence

$$e_n(t) = \sum_{j=0}^{n} \varepsilon_{n-j}\, \phi_j(t/h) + \mathcal{O}(h^2) \tag{3.11}$$

and it remains to bound the ε_j. To do this we follow [7] and note that

$$\sum_{j=0}^{n} \frac{q_j}{h}\, \varepsilon_{n-j} = \sum_{j=0}^{n} \frac{q_j}{h}\, u(t_{n-j}) - \frac{1}{h} \int_0^{t_n} K(t)\, u(t_n - t)\, dt := R_n\,. \tag{3.12}$$

After some tedious technical manipulation it can be shown that

$$R_{n+1} - 2\, R_n + R_{n-1} = \mathcal{O}(h^3)$$

and taking the second central difference of the expression (3.12) then gives

$$\sum_{j=0}^{n} \beta_j\, \varepsilon_{n+1-j} = \mathcal{O}(h^3)\,,$$

where $\beta_j := (q_j - 2\, q_{j-1} + q_{j-2})\,/h$ for $j \ge 0$, and we set $q_{-1} = q_{-2} = 0$. Note that the β_j are the coefficients of p_{n+1-j} in (3.2) scaled by h. It follows from Taylor expanding K and using P4 from Lemma 2.4 (and much simplification) that there is a constant C independent of h such that

$$\left| \beta_j - \overline{\beta}_j \right| \le C \begin{cases} h & \text{when } j = 0:1, \\ h\, e^{-\alpha^2 (j-2)^2} + h^2 & \text{when } j = 2:N_T, \end{cases}$$

where $\overline{\beta}_j = \beta_j|_{K \equiv 1}$. It was shown in the proof of Lemma 3.1 that $\overline{\beta}_0 > 0$ and $\overline{\beta}_j < 0$ for $j \ge 1$ if $\alpha > 1.2$, and a similar argument to that used in the proof of Theorem 3.1 gives the bound

$$|\varepsilon_{n+1}| \le (1 + Ch) \max_{j=0:n} |\varepsilon_j| + C\, h^3 \quad \text{for } n \le N_T$$

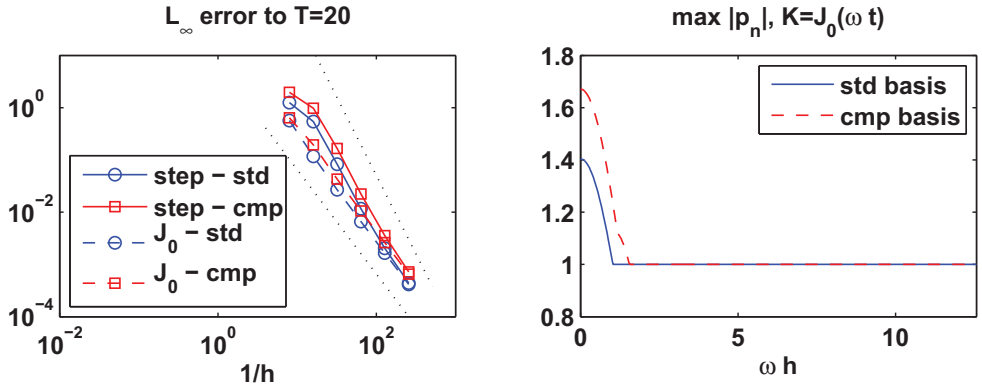

FIG. 3.2. *Left: L_∞ error vs. h for the VIE with step-function kernel K_L (with $L = \sqrt{0.9}$) and Bessel function kernel $K(t) = J_0(\omega t)$ (with $\omega = 1$) computed using basis functions ϕ_j with $\alpha = \sqrt{2}$ (std) and the compact basis functions derived from $\tilde{\psi}$ (cmp). The dotted lines show convergence of orders two and three. Right: Plot of $\max_{n\le 1000} |p_n|$ against ω for $\omega \in (0, 12/h)$ for the Bessel function kernel for both sets of basis functions.*

for a constant C independent of h. Hence

$$|\varepsilon_n| \le C\, h^3 \sum_{k=0}^{n-1} (1 + C\, h)^k < e^{CT}\, h^2$$

when $n \le N_T$. Substituting this into (3.11) and using P2 of Lemma 2.4 gives (3.10), which concludes the proof. ∎

Numerical convergence and stability for the VIE with step-function kernel and Bessel function kernel $K(t) = J_0(\omega t)$ are illustrated in Figure 3.2. The numerical results have been computed using the basis functions ϕ_j (labeled "std") and those derived from $\tilde{\psi}$ of (2.13) (labeled "cmp"). The right-hand plot shows $\max_{n\le 1000} |p_n|$ against frequency ω up to $\omega = 12/h$ for the Bessel function kernel for both sets of basis functions. The curved parts at the left correspond to $|p_1| > 1$.

4. Convolution-in-time approximation of the TDBIE. We report on numerical tests approximating the solution of the TDBIE (1.1) with piecewise constant spatial basis functions on a generally irregular triangular grid and report on the new temporal approximation introduced in section 2. The solution is approximated by

$$u(\boldsymbol{x}, t_n - t') \approx \sum_{j=0}^{n} \sum_{k=1}^{M} u_k^{n-j} \phi_j(t'/h)\, \eta_k(\boldsymbol{x}),$$

where

$$\eta_k(\boldsymbol{x}) = \begin{cases} 1 & \text{for } \boldsymbol{x} \in \Omega_k, \\ 0 & \text{otherwise} \end{cases}$$

and Ω_k is the kth triangle on the surface Γ. We consider both collocation and Galerkin approximations in space with the convolution-in-time approximation and both cases result in the time marching scheme

$$\mathsf{Q}^0\, \underline{U}^n = \underline{a}^n - \sum_{m=1}^{n} \mathsf{Q}^m\, \underline{U}^{n-m},$$

where $\underline{U}^n = (u_1^n, \ldots, u_M^n)^T$ and the coefficient matrices Q^m are defined below. The scheme is well defined when Q^0 is nonsingular.

Collocation in space at the element midpoints $\boldsymbol{x}_j$ gives system matrices Q^m and incident field vectors $\underline{a}^n$ with elements

$$\mathsf{Q}^m_{j,k} = \int_{\Omega_k} \frac{\phi_m(|\boldsymbol{x} - \boldsymbol{x}_j|/h)}{|\boldsymbol{x} - \boldsymbol{x}_j|}\, d\boldsymbol{x}, \quad a_j^n = a(\boldsymbol{x}_j, t^n)\,,$$

and Galerkin in space gives elements

$$\mathsf{Q}^m_{j,k} = \iint_{\Omega_j \times \Omega_k} \frac{\phi_m(|\boldsymbol{x} - \boldsymbol{y}|/h)}{|\boldsymbol{x} - \boldsymbol{y}|}\, d\boldsymbol{x}\, d\boldsymbol{y}, \quad a_j^n = \int_{\Omega_j} a(\boldsymbol{x}, t^n)\, d\boldsymbol{x}\,.$$

In both cases a cutoff is applied when ϕ_m is small. The collocation matrices are not symmetric and involve only two-dimensional integrals. The Galerkin matrices are symmetric, and each calculation involves a four-dimensional integral. In both cases the off-diagonal elements of Q involve integrals with smooth integrands so that standard quadrature methods can be used. The diagonal elements have a singular integrand and we use a Duffy-type transformation to convert them into smooth subintegrals, which are then approximated by quadrature of the same accuracy as the rest of the calculation.

In the numerical tests below we use the following quadrature methods to approximate the integrals in Q^m and $\underline{a}^n$. For triangular elements we use a composite triangular quadrature with 16 subtriangles, each of which is fourth order with six quadrature points. We use the parameter $\alpha = \sqrt{2}$ in the standard basis functions ϕ_j and choose h in all tests such that it is approximately half the size of a typical space mesh element Δx. We consider three types of surface: Γ is a flat plate, an open or closed cube, and a sphere.

4.1. Flat plates. We consider scattering from a flat square plate of unit size and from a flat, nonconvex polygonal plate (i.e., a screen problem). Both plates lie in the plane $z = 0$ and the square is $(x_1, x_2) \in [0,1] \times [0,1]$, while the polygon shown in Figure 4.1 is in roughly the same location. The incident field is a spherical wave originating at $\boldsymbol{x}_0 = (-5, -5, -5)$ with

$$a(\boldsymbol{x}, t) = \frac{a_0(t + t_0 - |\boldsymbol{x} - \boldsymbol{x}_0|)}{|\boldsymbol{x} - \boldsymbol{x}_0|}\,, \tag{4.1}$$

where

$$t_0 = \min_{\boldsymbol{x} \in \Gamma} |\boldsymbol{x} - \boldsymbol{x}_0| \quad \text{and} \quad a_0(t) = \begin{cases} 0 & \text{for } t \le 0, \\ t^2 \exp(-20(t - 1/2)^2) & \text{for } t > 0. \end{cases}$$

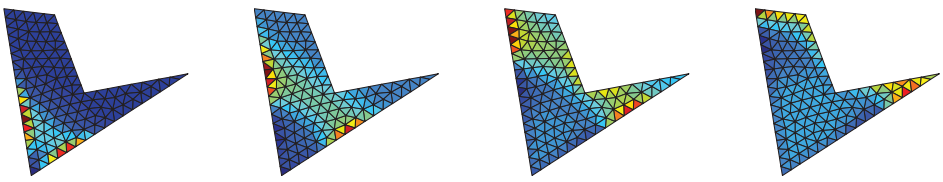

FIG. 4.1. *The approximate solution using collocation on a polygonal flat plate. The snapshots are* 0.25 *time units apart moving from left to right, and there are* 228 *elements on the plate.*

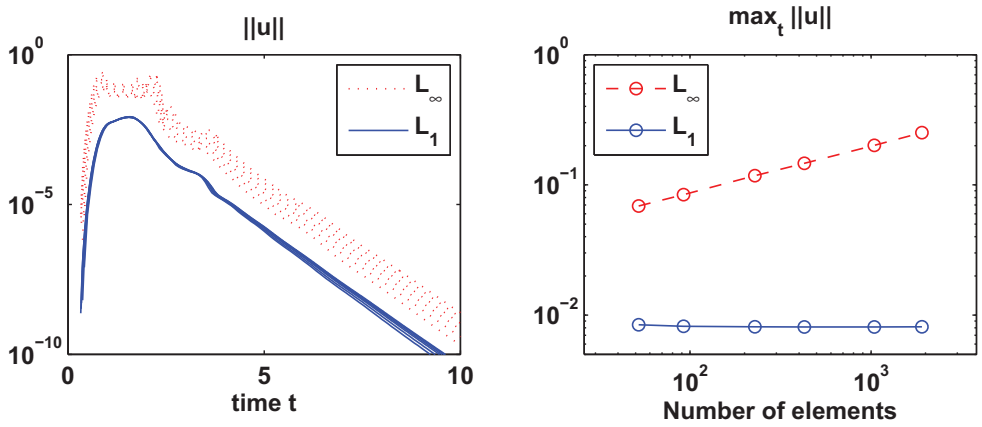

FIG. 4.2. *Behavior of the approximate solution using collocation on a polygonal flat plate. The left plot shows superimposed results for a range of difference mesh sizes, and the right plot shows the maximum values from each result on the left plot.*

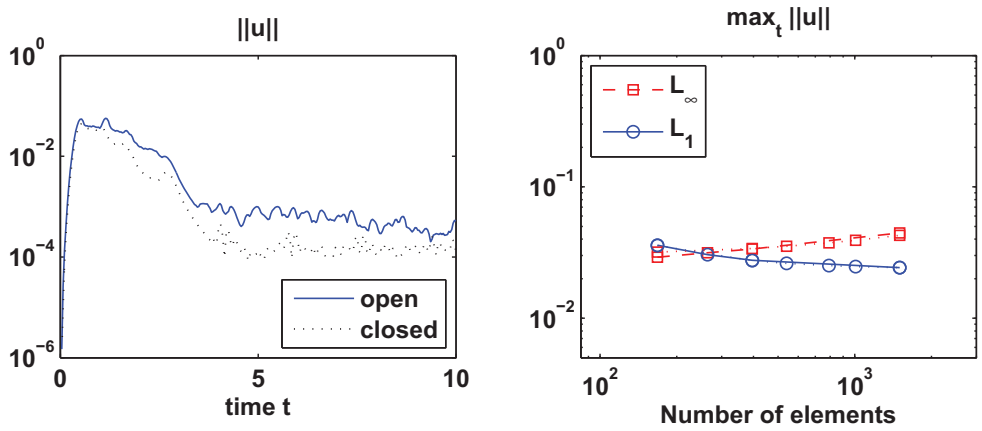

FIG. 4.3. *Behavior of the approximate solution using the Galerkin approximation on both a closed cube and an open box (the cube surface with one face missing). The left plot shows L_∞ norm results with 250 elements per face on the cube, and the right plot shows the maximum L_∞ and L_1 values for different meshes for both open and closed cubes, which are almost indistinguishable here.*

Figure 4.1 shows a time sequence of the approximate solution on the polygonal plate as the incident spherical wave progresses. We see in Figure 4.2 that this test appears completely stable in the L_1 norm as the mesh is refined for collocation on the polygonal plate. On the other hand, the L_∞ results show an increase in size as the mesh is refined. This is expected since there are singularities at the corners of the domain (see, e.g., [12]). The results look very similar for collocation and Galerkin space approximations on both the square and polygonal plates, and so we show only one case here.

4.2. Open and closed cubes. These tests show results for the surface of the unit cube $[0,1] \times [0,1] \times [0,1]$ in two cases: one completely closed and the other open with one side missing. The incident field is again given by (4.1). Again all the results appear completely stable and typical results are shown in Figure 4.3.

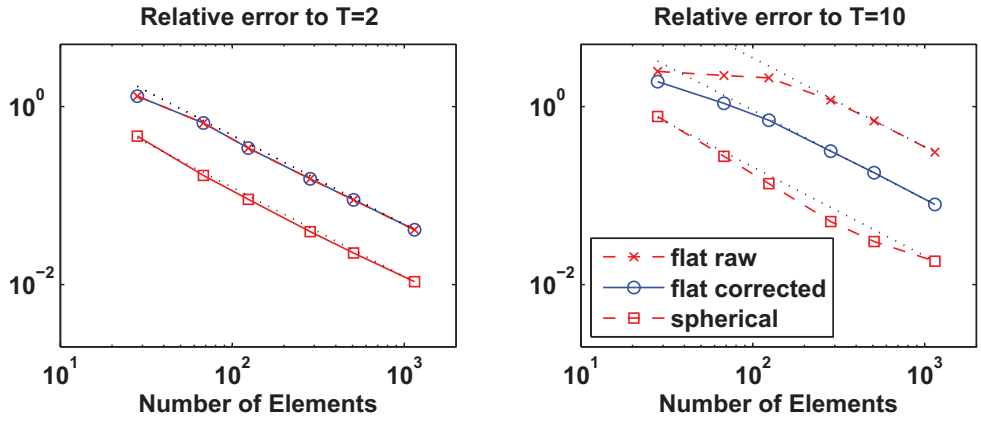

FIG. 4.4. *Error in scattering from a sphere in the spatial Galerkin case. The L_∞ error shown is normalized by the maximum modulus exact solution value* (4.2). *"Flat" refers to a flat triangle polyhedral approximation of the unit sphere, while "spherical" indicates that a coordinate transformation is used to give curved triangular elements lying exactly on the sphere surface.*

4.3. Unit sphere. This time we look at scattering from the unit sphere $|\boldsymbol{x}| = 1$ with incident field a given by (4.1) with $\boldsymbol{x}_0 = 0$. This problem has the exact solution (see [18]) on the sphere's surface

$$u(\boldsymbol{x}, t) = \sum_{k=0}^{\lfloor (t+t_0-1)/d_s \rfloor} a_0'(t + t_0 - 1 - kd_s), \tag{4.2}$$

where the sphere diameter is $d_s = 2$.

Figure 4.4 shows the L_∞ error for the spatial Galerkin scheme normalized by the maximum modulus exact solution value versus the total number of elements of reasonably uniform size (representative diameter Δx) used to model the sphere. The "flat" results are for the polyhedron constructed from flat triangles with nodes exactly on the surface of the unit sphere. "Flat raw" uses the diameter $d_s = 2$ in the exact solution (4.2), while "flat corrected" uses the slightly smaller value corresponding to the sphere radius with the same area as the polyhedron. Finally, in the same figure we show the result of using a coordinate transformation to work with curved spherical triangles lying exactly on the sphere's surface. These results all eventually show $\mathcal{O}(\Delta x^2)$ convergence, but the "flat raw" results deteriorate after only a few time periods. Clearly the coordinate transformation gives the best results, and this is a worthwhile modification because the extra computational cost is relatively small.

Figure 4.5 shows a comparison between the BDF2 convolution quadrature method and our standard basis functions for this sphere scattering problem, both using Galerkin in space. There is good agreement between the two methods and the exact solution for time $t \leq 2$, but the BDF2 results deteriorate drastically after that when the finite diameter of the sphere becomes important. The wider support of the BDF2 basis functions makes the system matrices denser than those for the ϕ_j, and so they are more expensive to set up and compute with. On this relatively coarse mesh with 508 elements, the computer time was about 3.6 times greater for BDF2 (and the results much worse), and this factor increases as the mesh is refined. Further tests over the same range of mesh sizes as in Figure 4.4 show that the two schemes have almost identical errors converging at $\mathcal{O}(\Delta x^2)$ in the initial period $t \in [0, 2]$, but

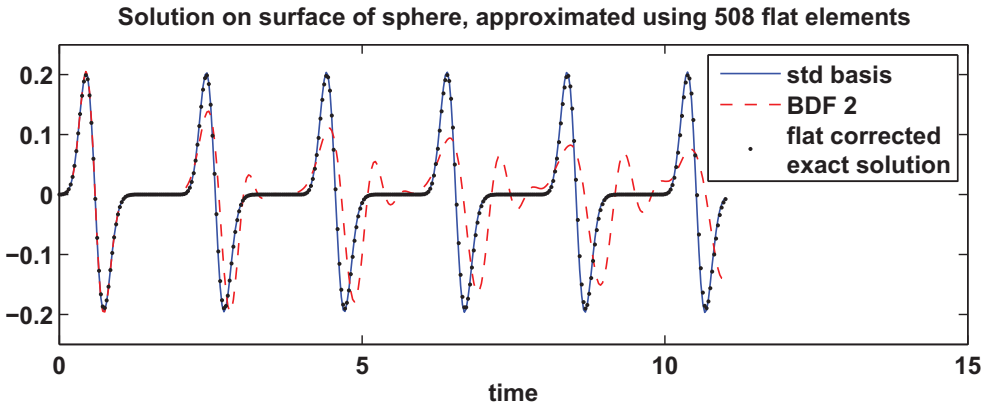

FIG. 4.5. *Results from our standard basis functions and BDF2 convolution quadrature method, both using Galerkin in space with piecewise constant elements. The exact solution is corrected to compensate for the polyhedral approximation of the sphere as in Figure* 4.4.

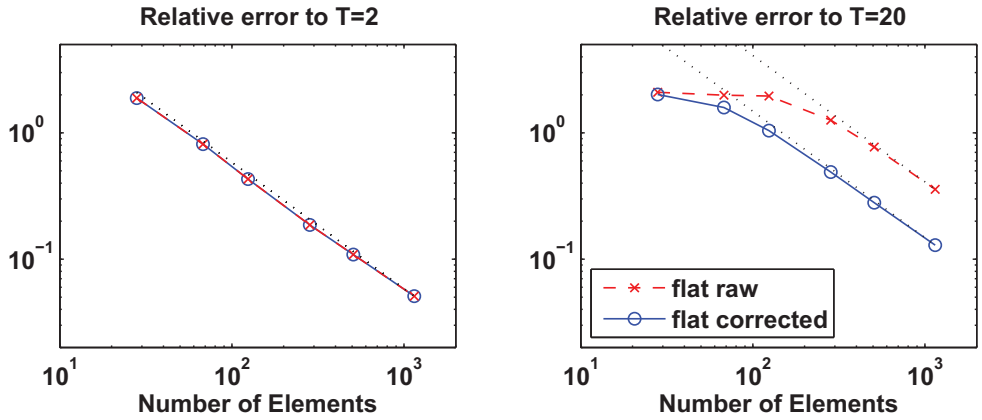

FIG. 4.6. *Error in scattering from a sphere in the spatial collocation case, using the compact temporal basis functions derived from* $\tilde{\psi}$ *of* (2.13). *The terms "flat raw" and "corrected" are as for Figure* 4.4.

as we have seen, over longer time intervals BDF2 performs poorly compared to our basis functions and many more space elements are required before it shows $\mathcal{O}(\Delta x^2)$ convergence.

We note that for this test problem using the standard time basis functions with piecewise constant element Galerkin in space appears completely stable in all the numerical tests (up to $T = 50$), but the spatial collocation approximation exhibits instability when the mesh is refined to more than about 100 elements. However, the compact basis functions derived from $\tilde{\psi}$ of (2.13) appear to give a stable scheme with collocation in space, as illustrated in Figure 4.6. The second order behavior is clear again, and the results are similar to those obtained using spatial Galerkin and time-basis functions ϕ_j.

5. Conclusions. The analysis of section 3 shows that the approximation scheme (1.3) has good stability properties for the VIE (1.2) and converges to the exact solution if the kernel and data are smooth enough. Our numerical tests indicate that it also

works well as a temporal approximation of the TDBIE (1.1): it appears stable in all the test problems we have looked at (from open and closed surfaces Γ) when combined with Galerkin in space. When a spatial collocation approximation is used, then the new scheme appears to be stable on open surfaces Γ, but it does exhibit instability on a unit sphere when the mesh is refined to more than about 100 elements. The advantage of using collocation in space is that it is cheaper to set up than Galerkin, but obviously a method which may be unstable is not reliable or robust enough to use for realistic simulations.

However, preliminary results for the compact basis functions derived from $\tilde{\psi}$ of (2.13) appear to indicate that they give a stable scheme for (1.1) with collocation in space, even on a sphere. They also have some other advantages over the basis functions ϕ_j: the setup costs for the coefficient matrices are lower since there are fewer elements to compute, and using sparser system matrices Q^m more than halves the execution time on a fine mesh. Clearly the compact basis functions are worthy of further investigation and analysis, and this is the focus of current work.

REFERENCES

[1] A. Bamberger and T. Ha Duong, *Formulation variationnelle espace–temps pour le calcul par potentiel retardé de la diffraction d'une onde acoustique* (I), Math. Methods Appl. Sci., 8 (1986), pp. 405–435.

[2] L. Banjai, *Multistep and multistage convolution quadrature for the wave equation: Algorithms and experiments*, SIAM J. Sci. Comput., 32 (2010), pp. 2964–2994.

[3] L. Banjai and Ch. Lubich, *An error analysis of Runge-Kutta convolution quadrature*, BIT, 51 (2011), pp. 483–496.

[4] L. Banjai, Ch. Lubich, and J. M. Melenk, *Runge-Kutta convolution quadrature for operators arising in wave propagation*, Numer. Math., 119 (2011), pp. 1–20.

[5] H. Brunner, *Collocation Methods for Volterra Integral and Related Functional Equations*, Cambridge University Press, Cambridge, UK, 2004.

[6] P. J. Davies and D. B. Duncan, *Stability and convergence of collocation schemes for retarded potential integral equations*, SIAM J. Numer. Anal., 42 (2004), pp. 1167–1188.

[7] P. J. Davies and D. B. Duncan, *Convolution Spline Approximations of Volterra Integral Equations*, www.mathstat.strath.ac.uk/research/reports/2012 (2012).

[8] I. S. Gradshteyn and I. M. Ryzhik, *Table of Integrals, Series, and Products*, 5th ed., Academic Press, Boston, 1994.

[9] T. Ha-Duong, *On the transient acoustic scattering by a flat object*, Japan J. Appl. Math., 7 (1990), pp. 489–513.

[10] T. Ha-Duong, *On retarded potential boundary integral equations and their discretisation*, in Topics in Computational Wave Propagation: Direct and Inverse Problems, M. Ainsworth, P. J. Davies, D. B. Duncan, P. A. Martin, and B. P. Rynne, eds., Springer-Verlag, Berlin, 2003, pp. 301–336.

[11] W. Hackbusch, W. Kress, and S. A. Sauter, *Sparse convolution quadrature for time domain boundary integral formulations of the wave equation*, IMA J. Numer. Anal., 29 (2009), pp. 158–179.

[12] H. Holm, M. Maischak, and E. P. Stephan, *The hp-version of the boundary element method for Helmholtz screen problems*, Computing, 57 (1996), pp. 105–134.

[13] W. Kress and S. A. Sauter, *Numerical treatment of retarded boundary integral equations by sparse panel clustering*, IMA J. Numer. Anal., 28 (2008), pp. 162–185.

[14] Ch. Lubich, *Convolution quadrature and discretized operational calculus.* I, Numer. Math., 52 (1988), pp. 129–145.

[15] Ch. Lubich, *On the multistep time discretization of linear initial–boundary value problems and their boundary integral equations*, Numer. Math., 67 (1994), pp. 365–389.

[16] F. W. J. Olver, D. W. Lozier, R. E. Boisvert, and C. W. Clark, *NIST Handbook of Mathematical Functions*, Cambridge University Press, Cambridge, UK, 2010.

[17] S. Sauter and A. Veit, *Adaptive Time Discretization for Retarded Potentials*, Preprint 04-2011, Institut für Mathematik, University of Zurich, 2011.

[18] S. Sauter and A. Veit, *A Galerkin Method for Retarded Boundary Integral Equations with Smooth and Compactly Supported Temporal Basis Functions. Part* II: *Implementation and Reference Solutions*, Preprint 03-2011, Institut für Mathematik, University of Zurich, 2011.
[19] I. Terrasse, *Résolution Mathématique et Numérique des Équations de Maxwell Instationnaires par Une Méthode de Potentials Retardés*, Thèse de l'École Polytechnique, 1993.
[20] H. Wendland, *Scattered Data Approximation*, Cambridge University Press, Cambridge, UK, 2010.
[21] W. Zongmin and R. Schaback, *Shape preserving properties and convergence of univariate multiquadric quasi-interpolation*, Acta Math. Appl. Sin., 10 (1994), pp. 441–446.